Pyroxene orientation within the upper mantle

NIKOLAS I. CHRISTENSEN
SUSAN M. LUNDQUIST
Department of Geological Sciences and Graduate Program in Geophysics, University of Washington, Seattle, Washington 98195

ABSTRACT

Petrofabric analyses of orthopyroxene and olivine for a suite of rocks from the Bay of Islands ophiolite, Newfoundland, show systematic relationships between the minerals' fabrics, the plane of the Mohorovičić discontinuity determined from the contact of the gabbro and ultramafic sections, and the spreading direction inferred from the attitude of the sheeted dikes. The orthopyroxene *c* crystallographic axes maxima, which are aligned subparallel to the spreading direction, coincide with olivine *a* axes maxima. The orthopyroxene *b* axes and olivine *c* axes also lie approximately within the plane of the Mohorovičić discontinuity but parallel the ridge, whereas the orthopyroxene *a* axes maxima and olivine *b* axes maxima are approximately perpendicular to the Mohorovičić discontinuity. Using olivine and orthopyroxene elastic constants and their pressure derivatives, velocities have been calculated from composite petrofabric data and contoured for varying proportions of olivine and pyroxene. The results of these calculations show that within a vertical direction compressional wave velocities change only slightly with increasing pyroxene content, whereas parallel to the Mohorovičić discontinuity velocities decrease with increasing pyroxene content. Anisotropy decreases from 4% for a rock with 100% olivine to 2.6% for a rock with 50% olivine and 50% orthopyroxene. Also within the plane of Mohorovičić discontinuity, the maximum and minumum velocities occur at approximately the same azimuth for differing percentages of orthopyroxene. A comparison of the calculated anisotropy and the observed seismic anisotropy off the coast of California shows a striking agreement. From this comparison, it is estimated that the percentage of orthopyroxene within the upper mantle of this region varies between 0% and 30%.

INTRODUCTION

One of the most significant observations pertaining to the nature of the upper mantle has been the recognition of widespread seismic anisotropy. Studies of P_n velocities from refraction data have clearly demonstrated that compressional wave velocities vary with azimuth beneath oceans (for example, Raitt and others, 1967, 1969; Morris and others, 1969) and continents (Bamford, 1977; Bamford and others, 1979). Laboratory studies of petrofabrics and velocity anisotropy in ultramafic rocks (for example, Birch, 1960; Christensen, 1966a, 1971; Babuska, 1972; Carter and others, 1972) have found that mantle anisotropy most likely originates from preferred orientation of olivine crystals. Compressional wave velocities within single crystal olivine range from a maximum of 9.89 km/s for propagation parallel to the *a* crystallographic axis to a minimum of 7.72 km/s for propagation along the *b* axis (Verma, 1960; Kumazawa and Anderson, 1969). Thus, wide ranges in anisotropy are possible in olivine aggregates, which depend upon the degree of preferred mineral orientation within the rock. Since preferred mineral orientation in tectonites is a consequence of stress, future detailed investigations of the existence and nature of anisotropy throughout the lithosphere promise to provide a wealth of information on tectonic processes that operate within the mantle.

Most models of anisotropy within the upper mantle have relied solely on olivine as being responsible for the observed variations of P_n velocities with azimuth (Hess, 1964; Francis, 1969; Christensen and Crosson, 1968; Crampin, 1977). In view of the dominance of olivine over other silicates in ultramafic rocks occurring as xenoliths and in the ultramafic levels of ophiolites, this assumption appears valid to a first approximation (Christensen and Salisbury, 1979). However, the widespread occurrence of orthopyroxene in rocks of probable mantle origin implies that it must also be a major component of the upper mantle. Observations of the phase mineralogy of peridotite nodules from alkali basalts (Ross and others, 1954), studies of ophiolites (for example, Smith, 1958), and models of upper-mantle composition (Ringwood, 1966) suggest an orthopyroxene content up to 40%. Clinopyroxenes are usually either absent or constitute only a few percent of the peridotites, and thus, they will not be considered in the discussions that follow.

The purposes of this paper are to provide information on the fabric of orthopyroxene within the upper mantle and assess the influence of preferred orthopyroxene orientation on upper-mantle seismic anisotropy. Petrofabric analyses of orthopyroxene are presented for field-oriented harzburgite specimens collected from the North Arm Massif of the Bay of Islands ophiolite, Newfoundland. An earlier study from the same massif (Christensen and Salisbury, 1979) has shown that for over 60 km[2] of ultramafic exposure the olivine fabrics are relatively uniform. Furthermore, the olivine *a* crystallographic axes are aligned approximately perpendicular to sheeted dikes within the complex, which results in a maximum velocity parallel to the inferred spreading direction, in excellent agreement with marine seismic observations. Velocity surfaces for the orthopyroxenes have been calculated at elevated pressures, and these have been combined with the olivine velocity surfaces to provide detailed anisotropy information for peridotite with various volume fractions of pyroxene and olivine.

PYROXENE PETROFABRICS

The Bay of Islands ophiolite, located in western Newfoundland, consists of four massifs containing typical ophiolite assem-

Geological Society of America Bulletin, v. 93, p. 279–288, 8 figs., 2 tables, April 1982.

blages (Fig. 1). The rocks comprising the massifs display a stratigraphy ranging from ultrabasic rocks with strong tectonite fabrics at the base through gabbros, a well developed sheeted dike complex, pillow basalts, and clastic sediments (Williams, 1971, 1973). The thickness and velocity structure for the mafic section of this sequence have been shown to be similar to normal oceanic crust determined from marine refraction studies (Salisbury and Christensen, 1978). This, in combination with the recognition of an ultramafic anisotropy pattern similar in magnitude and direction to that observed in oceanic upper mantle (Christensen and Salisbury, 1979), provides strong support that the complex is a segment of oceanic crust and upper mantle.

An investigation of the thin sections in which olivine fabrics were reported by Christensen and Salisbury (1979) showed that samples from eight localities within the ultramafic section of the North Arm Massif contained more than a few percent enstatite, the locations of which are illustrated in Figure 1. Because of the high degree of serpentinization (up to 70%), multiple thin sections were required to obtain sufficient numbers of enstatite grains for petrofabric analyses from these localities. The petrofabric patterns of enstatite are shown as Kamb plots in Figure 2. The fabrics were determined by standard procedures, using a five-axis universal stage (Emmons, 1943).

Composite fabric diagrams for the eight localities are shown in Figure 3. Orientation data for 800 olivine crystals and 530 orthopyroxene crystals were used for constructing the diagrams. Also shown in Figure 3 are the approximate attitudes of the sheeted dikes and the boundary between the gabbros and ultramafics (the Mohorovičić discontinuity). The strikes of the sheeted dikes generally trend from northwest to north-northwest (Williams, 1973; Christensen and Salisbury, 1979).

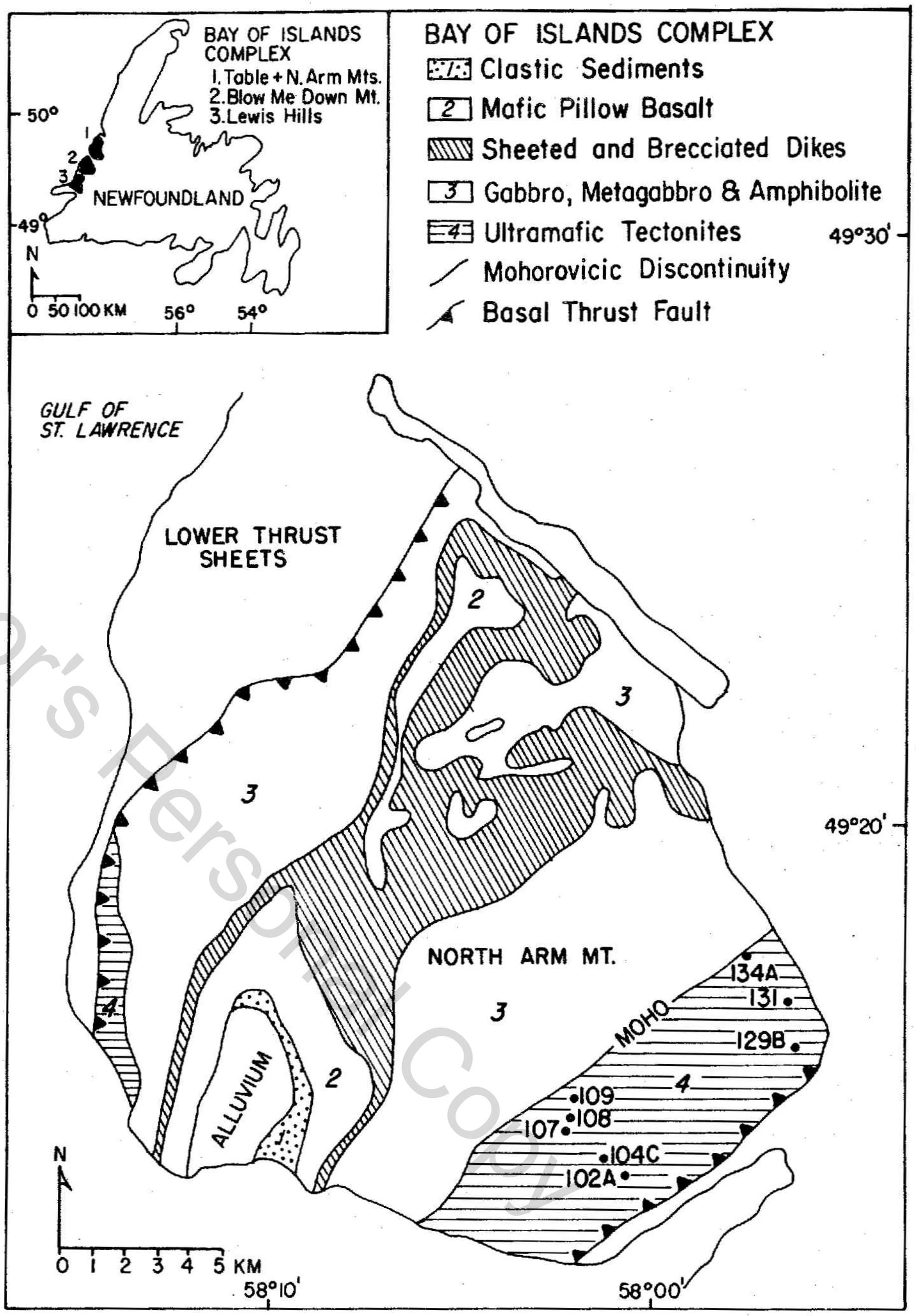

Figure 1. Location of samples used for petrofabric studies from the North Arm Massif, Bay of Islands Ophiolite, Newfoundland (map after Williams, 1971).

The following conclusions can be drawn from the orthopyroxene and olivine orientation data:

1. Although preferentially oriented, the orthopyroxene crystallographic axes do not possess as strong concentrations as those of olivine.

2. The orthopyroxene *a* axes show well-developed maxima, which tend to lie in a horizontal plane and strike NW-SE or dip at shallow angles to the SE. The orientations of the *b* axes are relatively weak and variable. The orthopyroxene *c* axes generally dip to the NE at moderate angles or are nearly horizontal with a NE-SW strike.

3. The olivine and orthopyroxene fabrics are systematically relatec to one another, with olivine *a* axes parallel or nearly parallel to orthopyroxene *c* axes and olivine *b* axes parallel to orthopyroxene *a* axes.

4. The olivine *a* and orthopyroxene *c* axes maxima lie within the plane of the Mohorovičić discontinuity and trend nearly parallel to the spreading direction inferred by the orientation of the sheeted dikes. The olivine *c* and orthopyroxene *b* axes also tend to lie within the Mohorovičić discontinuity. The olivine *b* and orthopyroxene *a* axes, on the other hand, show well-developed maxima normal to the Mohorovičić discontinuity (that is, within the oceanic upper mantle, these axes would be vertical or nearly vertical).

MANTLE SEISMIC ANISOTROPY

An examination of previous literature dealing with the relationship of olivine orientation to that of enstatite (Table 1) shows that several possible combinations, including both symmetric and nonsymme-

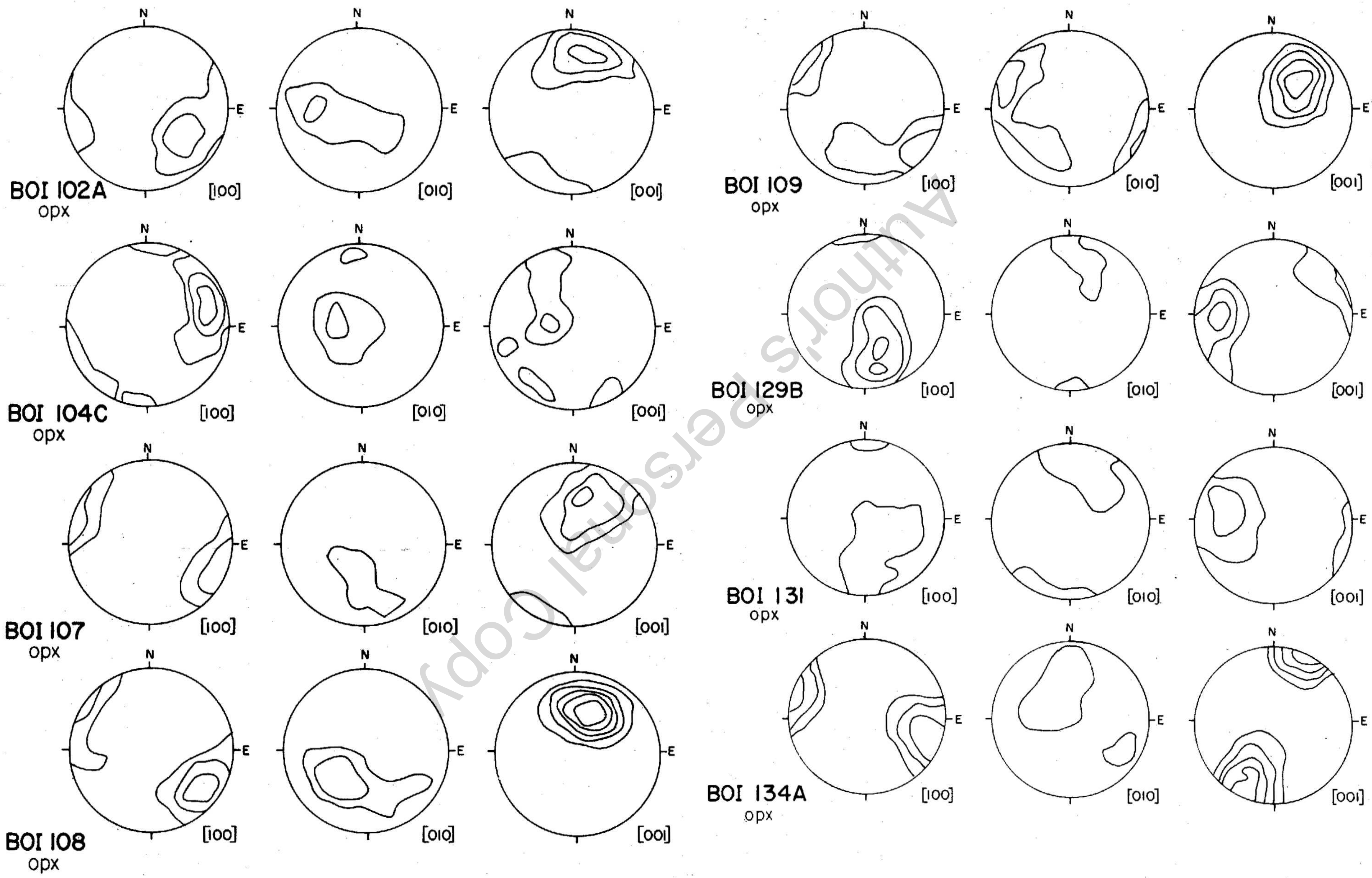

Figure 2. Equal-area, lower-hemisphere projections of [100], [010], and [001] axes of orthopyroxene plotted as Kamb diagrams for samples 102A, 104C, 107, 108, 109, 129B, 131, and 134A, from the North Arm Massif. N ranges from 50 to 90 for each sample; projection contoured in 2σ intervals with the lowest contour = 4σ; σ = 2.75; E = 3σ; counting area A = 0.083.

tric, are found in ultramafic rocks. This is not surprising considering the various mechanisms that produce preferred mineral orientation (for example, recrystallization, intracrystalline gliding, and crystal settling), the many possible origins of ultramafic rocks, the varying degrees of intensity of deformation that are possible, and the possibility that fabrics of some ultramafics have originated from multiple deformations. The crystallographic relationships found between olivine and orthopyroxene fall into three main categories:

1. The axes *a*, *b*, and *c* of orthopyroxene essentially correspond to *a*, *b*, and *c* axes of olivine, with minor deviations where the preferred orientation of an axis is weak.

2. The *c* axis of orthopyroxene parallels the *a* axis of olivine, with the othopyroxene *a* and *b* axes usually coinciding with *b* and *c* axes of olivine, respectively.

3. There is no significant relationship between the minerals' preferred orientations.

The olivine and enstatite fabrics observed for the Bay of Islands ultramafics appear to be quite common in ophiolites (Table 1) and

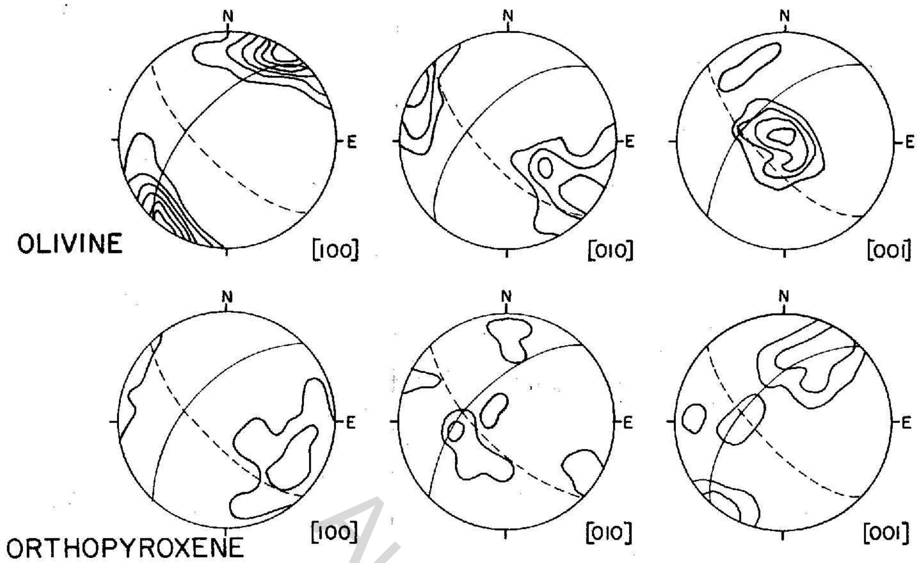

Figure 3. Composite olivine and orthopyroxene equal area, lower-hemisphere projections of [100], [010], and [001] axes plotted as Kamb diagrams for samples 102A, 104C, 107, 108, 109, 129B, 131, and 134A, from the North Arm Massif. N = 800 for the olivine diagram and 530 for the orthopyroxene diagram; projection contoured in 2σ intervals with the lowest contour = 4σ; $\sigma = 2.75$; E = 3σ; counting area A = 0.083. Dashed lines represent the attitude of the sheeted dikes, and solid great circles represent the attitude of the boundary between the gabbros and the ultramafics.

TABLE 1. RELATIONSHIPS OF ORTHOPYROXENE TO OLIVINE ORIENTATIONS FROM PETROFABRIC ANALYSES IN ULTRAMAFIC ROCKS

Reference	Rock type—Locality	Crystallographic relationships*	
Brothers and Rodgers, 1969	Foliated harzburgite nodule; Bridal Veil Falls, Auckland, New Zealand	$[100]_{opx} \cong [100]_{ol}$ $[001]_{opx} = [001]_{ol}$	
den Tex, 1969	Garnet peridotite; Alpe Arami, Switzerland (after J. R. Möckel, 1969)	$[100]_{opx} = [100]_{ol}$ $[001]_{opx} = [001]_{ol}$	Normal to primary layering In primary layering
Nicolas and others, 1971	Moderately deformed lherzolite; small recrystallized olivine grains; Lanzo Massif, Italian Alps	$[100]_{opx} = [010]_{ol}$ $[010]_{opx} \cong [100]_{ol}$ $[001]_{opx} = [001]_{ol}$	Normal to foliation Partial girdle in foliation In foliation
Carter and others, 1972	Results from syntectonic recrystallization experiments	$[100]_{opx} \cong [100]_{ol}$ $[010]_{opx} = [010]_{ol}$ $[001]_{opx} \cong [001]_{ol}$	
	Spinel lherzolite L-62; Etang de Lers, French Pyrenees	$[100]_{opx} = [100]_{ol}$ $[010]_{opx} = [010]_{ol}$ $[001]_{opx} = [001]_{ol}$	Maxima in foliation Maxima spreading into a girdle normal to foliation Partial girdles in foliation
Nicolas and others, 1971	Mildly deformed lherzolite; Lanzo Massif, Italian Alps	$[100]_{opx} = [010]_{ol}$ $[010]_{opx} = [001]_{ol}$ $[001]_{opx} = [100]_{ol}$	Normal to foliation Partial girdle in foliation Partial girdle in foliation $[100]_{ol}$ tends to interchange with $[001]_{ol}$
	Moderately deformed lherzolite; large kinked olivine grains; Lanzo Massif	$[100]_{opx} = [010]_{ol}$ $[010]_{opx} = [001]_{ol}$ $[001]_{opx} = [100]_{ol}$	Normal to foliation Partial girdle in foliation In foliation
	Strongly deformed lherzolite; Lanzo Massif	$[100]_{opx} = [010]_{ol}$ $[010]_{opx} \cong [001]_{ol}$ $[001]_{opx} = [100]_{ol}$	Normal to foliation Tends to form girdles, roughly in foliation In foliation
Carter and others, 1972	John Day lherzolite; Canyon Mountain Complex, Oregon (from H. G. Avé Lallemant, 1971, personal commun.)	$[100]_{opx} \cong [010]_{ol}$ $[010]_{opx} = [001]_{ol}$ $[001]_{opx} = [100]_{ol}$	Girdles Girdles Parallel, well-developed maxima

TABLE 1. *(Continued)*

Reference	Rock type—Locality	Crystallographic relationships*
Avé Lallemant, 1976	Lherzolite and foliated gabbro; Canyon Mountain Complex, Oregon	$[100]_{opx} = [010]_{ol}$ Girdles around lineation with weak concentrations of $[100]_{opx}$ and $[010]_{ol}$ normal to foliation $[010]_{opx} \cong [001]_{ol}$ Maxima parallel to lineation with partial girdle sub- $[001]_{opx} = [100]_{ol}$ parallel to foliation
	Foliated olivine pyroxenite; Canyon Mountain Complex	$[100]_{opx}$ and $[010]_{ol}$ Show a very weak correlation $[010]_{opx} \cong [001]_{ol}$ $[001]_{opx} = [100]_{ol}$
Loney and Himmelberg, 1976	Harzburgite; Vulcan Peak Peridotite, S.W. Oregon	$[100]_{opx} = [010]_{ol}$ Normal to foliation, S_1 $[010]_{opx} \cong [001]_{ol}$ $[001]_{opx} = [100]_{ol}$ Partial girdles parallel to S_1
Nicolas and Poirier, 1976	Feldspathic lherzolite; Lanzo Massif, Italian Alps (after Boudier, 1976)	$[100]_{opx} = [010]_{ol}$ Pole to the only slip plane $[010]_{opx} \cong [001]_{ol}$ $[001]_{opx} = [100]_{ol}$ Parallel to the only slip direction
	Mylonitic lherzolite; margin of the Lanzo Massif (after Boudier, 1976)	$[100]_{opx} = [010]_{ol}$ Slip direction parallel to lineation $[001]_{opx} = [100]_{ol}$ Parallel to foliation
	Lherzolite xenoliths in alkali basalts; Hawaii and Massif Central France (after Mercier, 1972 and Mercier and Nicolas, 1975); porphyroclastic and tabular equigranular textures	$[100]_{opx} = [010]_{ol}$ $[001]_{opx} = [100]_{ol}$
George, 1978	Harzburgite; Troodos Ophiolite, Cyprus	$[100]_{opx} \cong [010]_{ol}$ Tends to be normal to foliation $[001]_{opx} = [100]_{ol}$ Subparallel to pyroxene foliation
Nicolas and others, 1980	Harzburgite (KDA-2); Antalya Massif, western Turkey	$[001]_{opx}$ weakly correlated with $[100]_{ol}$—Maxima close to the mineral lineation
	Harzburgite (NOVA 88); dredge sample from Tonga Trench and harzburgite (140301-17); dredged from Marianas Trench	$[100]_{opx} \cong [010]_{ol}$ $[001]_{opx} = [100]_{ol}$
	Harzburgite (OMB-7); Samail Ophiolite, Oman	$[100]_{opx} \cong [010]_{ol}$ Weak correlation $[010]_{opx} \cong [001]_{ol}$ $[001]_{opx} \cong [100]_{ol}$ Weak correlation
Raleigh, 1965	Cypress peridotite; Cypress Island, Washington	No symmetrical relationship found between orthopyroxene and olivine fabrics
den Tex, 1969	Lherzolite pyroxenite nodule in alkali olivine basalt; Solignac-Plateau de Velay, France (after A.L.G. Collée, 1963)	$[100]_{opx}$ and $[010]_{ol}$ Partial girdles with maxima about 70° apart
Helmstaedt and Anderson, 1969	Lherzolite inclusion; Mule Ear and Garnet Ridge kimberlite pipes, southeastern Utah and northeastern Arizona	$[100]_{opx}$ shows a strong maxima not related to the olivine fabric $[001]_{opx}$ spreads into a broad girdle which contains the weak maxima of $[100]_{ol}$
Carter and others, 1972	Chlorite peridotite (AR-18); Alpe Arami, Switzerland (from J. R. Möckel, 1971, personal commun.)	Orthopyroxene fabric not at all related to the olivine fabric
Nicolas and Poirier, 1976	Lherzolite xenoliths in alkali basalts; Hawaii and Massif Central France (after Mercier, 1972, and Mercier and Nicolas, 1975); protogranular and mosaic equigranular textures	Orthopyroxene and olivine have weak to no preferred orientation
Nicolas and others, 1980	Harzburgite (OMB 43) from upper part of peridotite section; Samail Ophiolite, Oman	No consistent relationship between olivine and orthopyroxene fabrics
	Oceanic peridotite from IPOD drilling; Mid-Atlantic Ridge	Olivine and orthopyroxene have no preferred orientation

*For orthopyroxene: $[100] = \beta$, $[010] = \alpha$, $[001] = \gamma$
For olivine: $[100] = \gamma$, $[010] = \alpha$, $[001] = \beta$
(after Deer and others, 1976)

are found in peridotites showing moderate to strong deformation as evidenced by a study of the Lanzo Massif (Nicolas and others, 1971). The (010) plane of olivine and the (100) plane of enstatite lie in the foliation, with the crystallographic *a* of olivine and *c* of enstatite parallel or subparallel to spinel lineations. We have observed a similar relationship between olivine and orthopyroxene petrofabrics, foliation, and lineation in peridotites from the Red Hills ophiolite of New Zealand, the Troodos ophiolite in Cyprus, and the Samail ophiolite of Oman. Thus, there is widespread evidence from many peridotite massifs, widely believed to represent fragments of oceanic upper mantle now emplaced on land, that olivine and enstatite have fabrics symmetrically related to one another.

The observation that within ophiolites orthopyroxene *c* axes and *a* axes tend to parallel olivine *a* axes and *b* axes, respectively (Fig. 3), has important implications regarding the influence of orthopyroxene on upper mantle seismic anisotropy. Figure 4a illustrates the ideal orientation within the upper mantle of single crystals of olivine and orthopyroxene inferred from the sheeted dikes and the gabbro-peridotite contact observed in the North Arm Massif (Fig. 3). Also shown are compressional wave velocities along the crystallographic axes. In Figure 4b, individual mineral velocity surfaces illustrating the compressional and two shear-wave velocities in km/s are shown for propagation in a plane parallel to the Mohorovičić discontinuity (that is, (010) for olivine and (100) for orthopyroxene).

From the relationships in Figure 4, the following conclusions regarding upper-mantle seismic anisotropy can be drawn:

1. The maximum compressional wave velocity in orthopyroxene (along the *a* axis) parallels the minimum compressional wave velocity in olivine (along the *b* axis). Within the mantle, concentrations of these axes will tend to be vertical. An appreciable amount of orthopyroxene in the upper mantle with a high degree of preferred orientation could increase velocities for vertical compressional wave propagation. This is somewhat surprising, since isotropic aggregate velocities of pyroxene are significantly lower than those of olivine (Christensen, 1966a).

2. Compressional wave velocities propagating parallel to the Mohorovičić discontinuity (that is, approximately horizontal) will vary with azimuth depending upon the degree of mineral orientation and the percentage of orthopyroxene. This anisotropy is the normal two-dimensional anisotropy recorded by P_n velocity studies. The maximum possible anisotropy is 16% for an upper mantle consisting of 100% olivine, and 13.5% for a pyroxenite upper mantle.

3. Within the plane of the Mohorovičić discontinuity (that is, for P_n propagation), the maximum velocity resulting from preferred olivine orientation will parallel the maximum velocity produced by orthopyroxene orientation. This maximum compressional wave velocity parallels the spreading direction. Relatively low compressional wave velocities related to concentrations of olivine *c* axes and orthopyroxene *b* axes occur parallel to ridge crests as inferred from the sheeted dikes.

4. For all directions within the plane of the Mohorovičić discontinuity, two shear waves propagate with differing velocities (Fig. 4b). This acoustic birefringence has been well documented in studies of shear wave velocities in rocks with preferred mineral orientations (Christensen, 1966b, 1971). The difference in velocity between the two shear waves will be a minimum for propagation parallel to the spreading direction (that is, parallel to olivine *a* axes concentrations and orthopyroxene *c* axes concentrations).

Using the elastic constants and their pressure derivatives for olivine (Kumazawa and Anderson, 1969) and orthopyroxene (Frisillo and Barsch, 1972), velocities have been calculated for several directions and contoured for the composite petrofabric diagrams of Figure 3. We have used the technique described by Crosson and Lin (1971), which has been shown to produce calculated velocities in excellent agreement with laboratory-measured velocities. Similar calculations have been well documented by Kumazawa (1964), Klima and Babuska (1968), and Baker and Carter (1972).

The contoured velocity surfaces calculated at pressures of 2 kbars (the approximate pressure at the oceanic crust-mantle boundary) are shown in Figure 5 for an upper mantle with varying proportions of

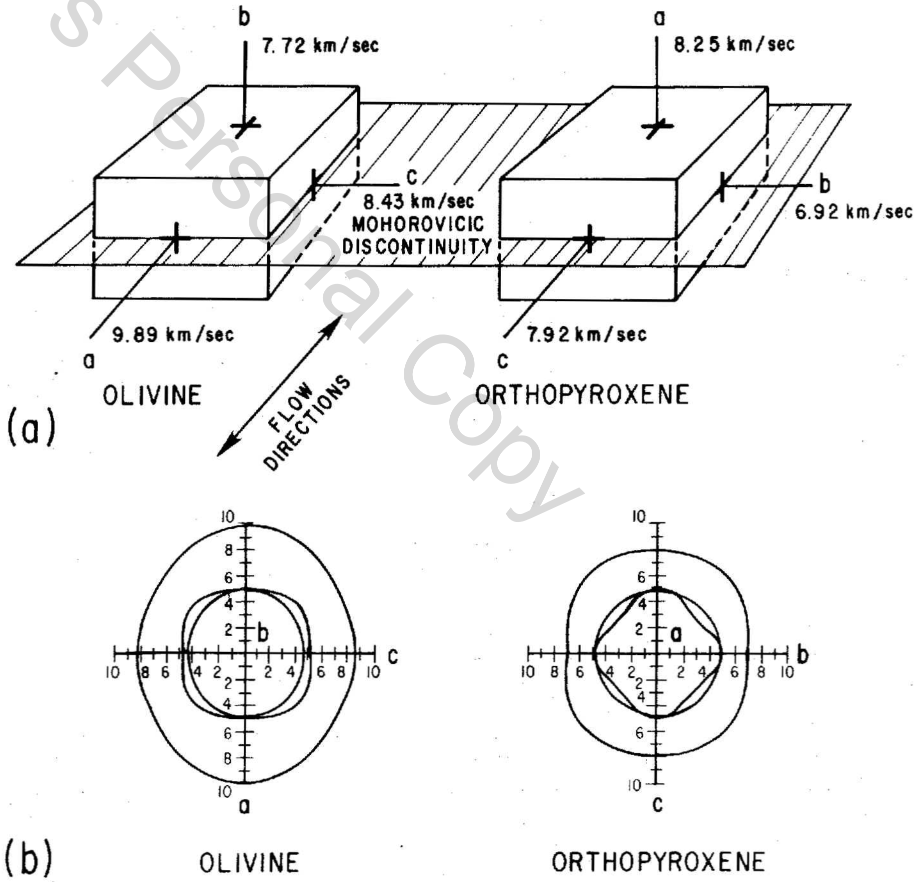

Figure 4. (a) Olivine and orthopyroxene orientations within the upper mantle. Single-crystal compressional wave velocities are for propagation along the crystallographic axes. (b) Compressional and shear velocities within the crystallographic olivine a–c plane and orthopyroxene b–c plane.

olivine and orthopyroxene. For all diagrams in this figure, the attitudes of the Mohorovičić discontinuity and sheeted dikes are the same as those given by the solid and dashed great circles in Figure 3. In addition to velocities, the difference in velocity between the two quasi-shear waves (ΔV_s) and the maximum and minimum values of Poisson's ratio (σ), calculated from the compressional and two shear-wave velocities, are contoured in Figure 5.

The contoured diagrams illustrate several features of seismic-wave propagation within the upper mantle:

1. As predicted above from the single-crystal measurements, the minimum compressional wave velocity for an olivine aggregate is normal to the Mohorovičić discontinuity, whereas the pyroxene aggregate has relatively high compressional wave velocities for this propagation direction.

2. For compressional wave propagation within the plane of the Mohorovičić discontinuity, maximum velocities are approximately parallel to the inferred spreading direction. It should be emphasized that in some regions of the oceanic upper mantle the maximum P_n velocities may deviate as much as 30° from the inferred spreading directions (for example, Raitt and others, 1971). Thus, for anisotropy studies of ophiolites it is not surprising to find maximum compressional wave velocities that depart from the spreading directions determined from sheeted-dike orientations. The anisotropy decreases from 4.1% for dunite with 100% olivine, to 2.4% for peridotite with 50% olivine and 50% orthopyroxene. The compressional wave velocities for a given propagation direction decrease with increasing pyroxene content.

3. Shear velocities also decrease with increasing pyroxene content. The shear-wave velocity anisotropy is small (<2%); however, ΔV_s is often greater than 4% with maximum values for propagation parallel to the ridge crest.

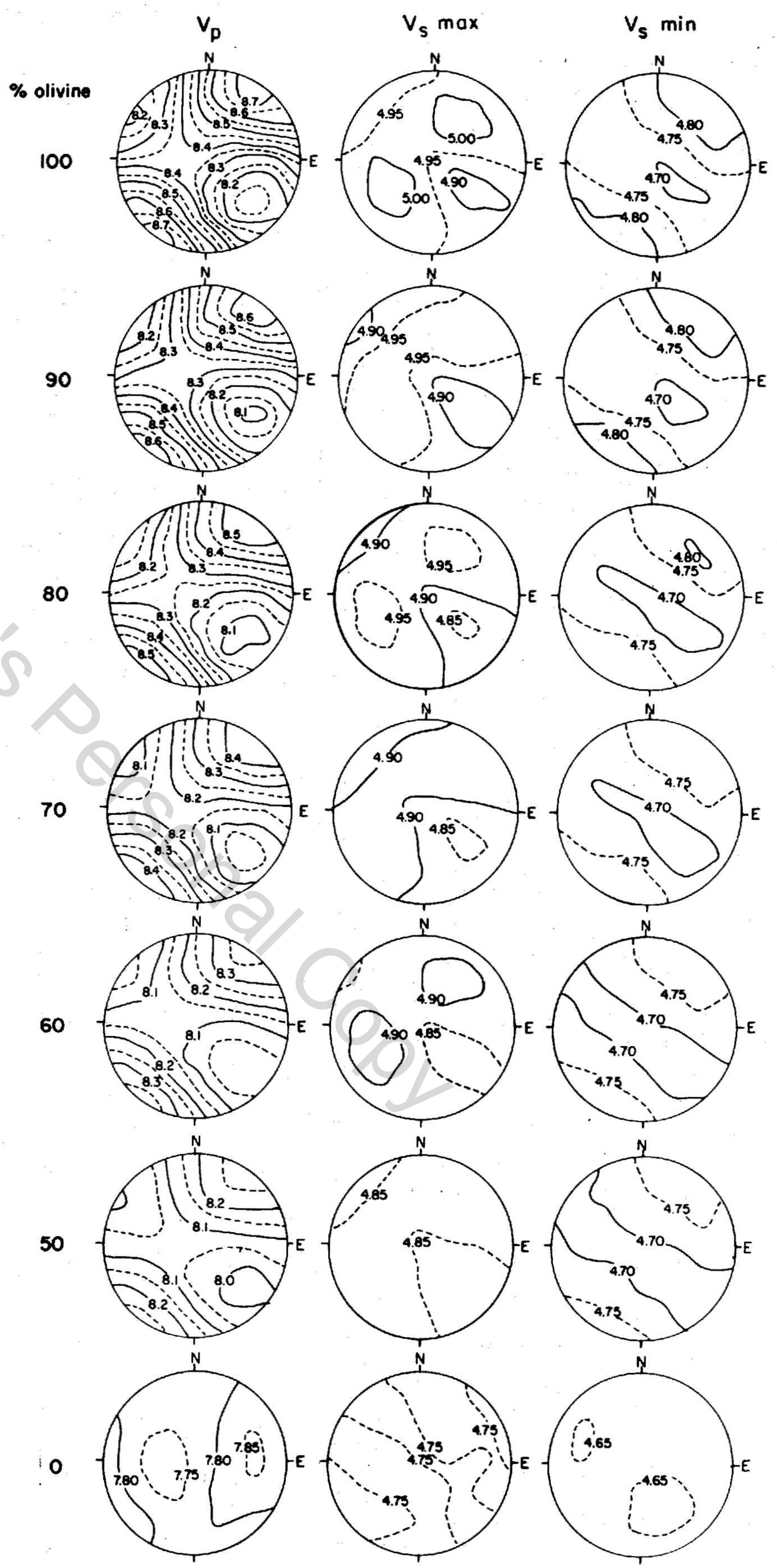

Figure 5. Variations in direction of compressional wave velocity (V_p), maximum shear-wave velocity ($V_{s_{max}}$), minimum shear-wave velocity ($V_{s_{min}}$), and the shear-wave dispersion (ΔV_s), all in km/s, along with Poisson's ratio (σ) based on $V_{s_{max}}$ and $V_{s_{min}}$ for varying proportions of olivine and orthopyroxene. (This figure is continued on following page.)

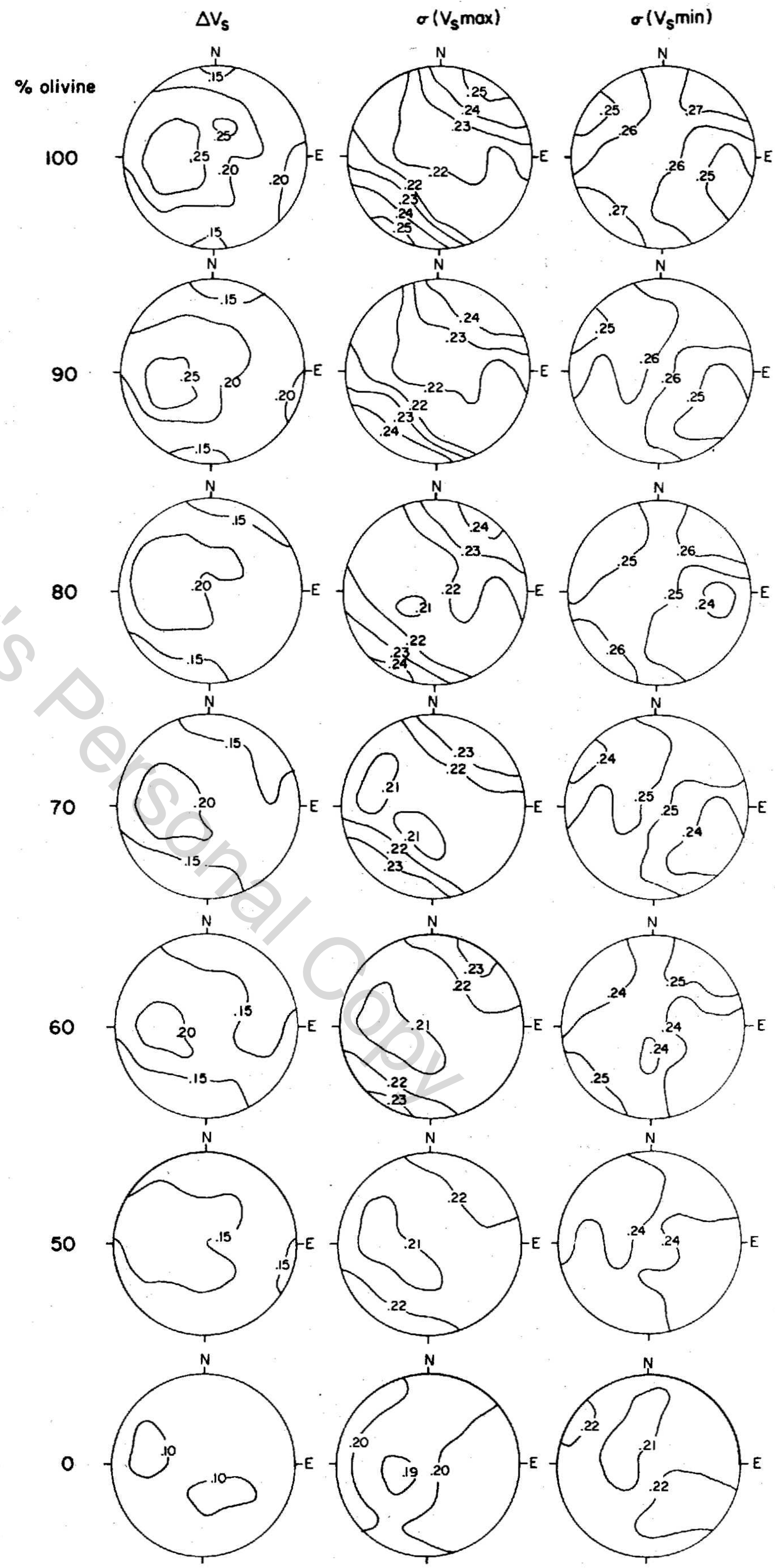

Figure 5. ***(Continued).***

4. Poisson's ratio decreases with increasing pyroxene content. For propagation within the plane of the Mohorovičić discontinuity, the maximum values of anisotropy of Poisson's ratio are those calculated from the maximum shear velocity. Also, maximum values of Poisson's ratio tend to parallel directions with maximum compressional wave velocities. (Strictly speaking, Poisson's ratios are calculated only for isotropic materials, and for anisotropic media the physical meaning of Poisson's ratio is vague at best. Thus it would perhaps be better to deal with ratios of V_p to V_s. However, in practice, Poisson's ratios are often presented from seismic-refraction data in which isotropy has not been demonstrated.)

Studies of anisotropy in the upper mantle have become more important with the increasing resolution of seismic observations. To date, most investigations have been limited to two-dimensional studies of compressional wave velocities in which the deviation from the mean velocity is plotted versus azimuth. This approach is particularly useful for comparisons with our calculated velocities, since the absolute values of velocity shown in Figure 5 are undoubtedly too high. The calculations have not taken into account the lowering of velocities produced by elevated upper-mantle temperature and the possible presence of accessory minerals, such as spinel, serpentine, and amphibole. However, although these factors would cause the velocities to be lowered, they will have little effect on the anisotropy. The presence of appreciable garnet in a peridotite upper mantle would, on the other hand, dilute the anisotropy (Carter and others, 1972) and maintain a relatively high velocity.

The calculated compressional velocities in the plane of the Mohorovičić discontinuity range over the values shown in Figure 6 for varying proportions of olivine. A mean velocity calculated for each modal percentage decreases from 8.54 km/s for an olivine content of 100%, to 8.16 km/s for a rock containing 50% olivine and 50% orthopyroxene. The azimuthal deviations from these mean values within the Mohorovičić discontinuity are plotted in Figure 7 at 10° intervals for rocks containing 100% olivine, 75% olivine–25% orthopyroxene, and 50% olivine–50% orthopyroxene. The min-

TABLE 2. LEAST-SQUARES SOLUTIONS TO THE BACKUS EQUATION FOR VARYING PYROXENE CONTENTS

Pyroxene (%)	V	B	C	E	F
0	8.54	−0.52	−2.86	0.15	0.08
10	8.47	−0.65	−2.52	0.13	0.10
20	8.39	−0.50	−2.25	0.08	0.06
30	8.31	−0.58	−2.08	0.02	0.01
40	8.24	−0.37	−1.92	0.10	−0.03
50	8.16	−0.48	−1.65	0.03	−0.04

imum velocities have been assigned azimuths of 0° (that is, propagation parallel to the crest for a north-south trending ridge).

Assuming small anisotropy (Backus, 1965), the equation relating azimuth (ϕ) to the velocity V_p is given by

$$V_p^2 = V_o^2 + B\cos 2\phi + C\sin 2\phi + E\cos 4\phi + F\sin 4\phi$$

where V_o is the mean velocity and B, C, E, and F are constants. Least-squares fits to the calculated data points are given in Table 2, and the resulting curves are shown in Figure 7. The curves for the various percentages of olivine are not symmetrical about the same axis, as the maxima shifts to a higher azimuth with increasing pyroxene content. Raitt and others (1971) have found from refraction data that the constants E and F of the 4ϕ terms in Backus' equation are statistically insignificant, which simplifies the above expression. This observation is further supported by our solutions in Table 2.

The magnitude of the anisotropy of the calculated compressional velocities in the plane of the Mohorovičić discontinuity also decreases with an increasing percentage of orthopyroxene (see Fig. 6). A rock with 100% olivine has 4.0% anisotropy, decreasing down to 2.6% for a rock with 50% olivine and 50% orthopyroxene. Higher anisotropies (up to 7.1% for an upper mantle consisting of 100% olivine) are possible for compressional wave propagation in a plane containing the olivine *a* and *b* axes maxima (Figs. 3 and 5). Upper-mantle anisotropies greater than 7.1% would require a higher degree of preferred olivine orientation and a relatively low pyroxene content (Figs. 4 and 5).

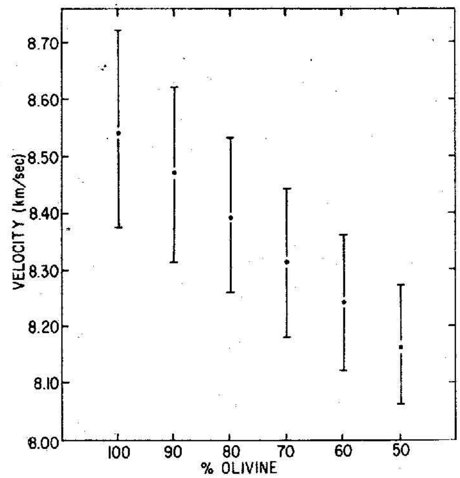

Figure 6. Ranges of calculated compressional velocities in the plane of the Mohorovičić discontinuity for varying proportions of olivine and orthopyroxene. Illustrated are decreases in mean velocity and the degree of anisotropy with increasing pyroxene content.

Finally, in Figure 8, we have included best least-squares fit curves for observed upper-mantle seismic anisotropy off the

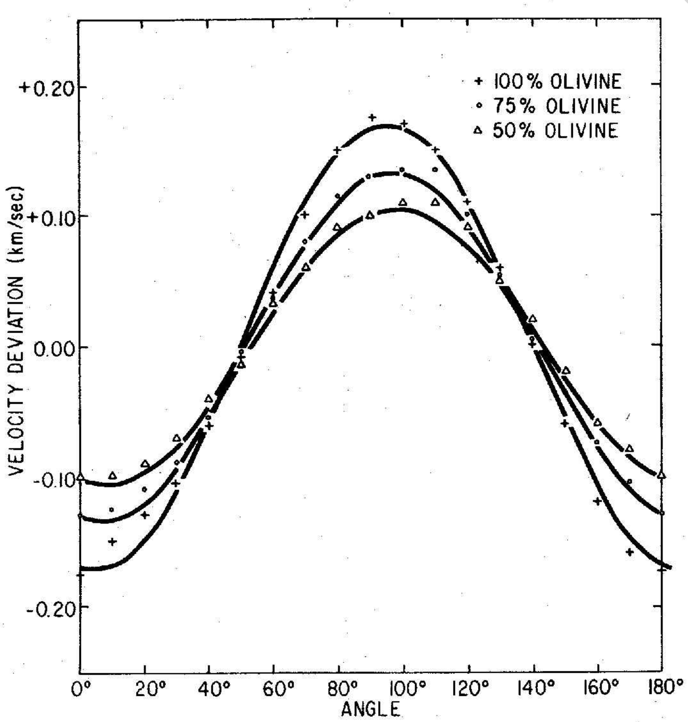

Figure 7. Anisotropy versus azimuth within the plane of the Mohorovičić discontinuity for varying proportions of olivine and orthopyroxene, using the calculated velocities shown in 5a. Inferred spreading direction is at 90°.

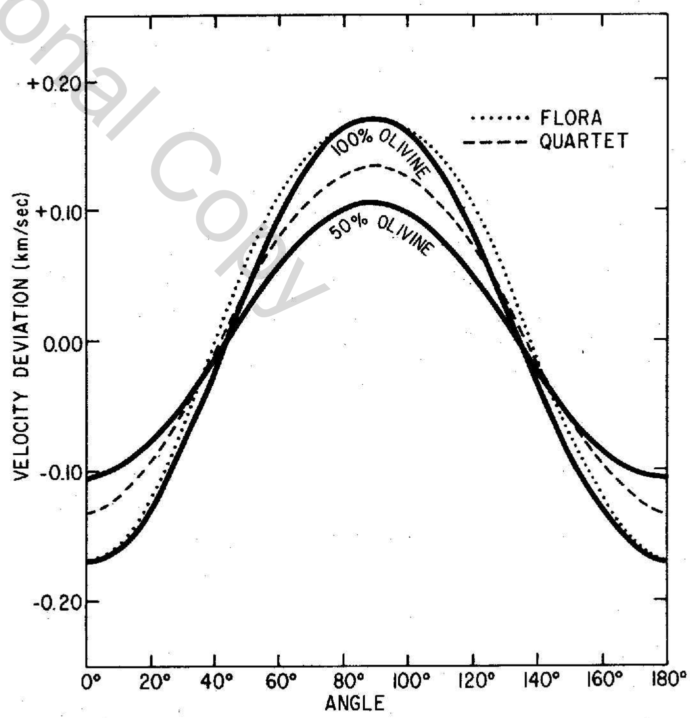

Figure 8. Comparison of upper-mantle seismic anisotropy from the Quartet and Flora areas (Raitt and others, 1967, 1969), with anisotropy calculated from petrofabric analyses of the ultramafic section in the Bay of Islands ophiolite.

coast of California from the Quartet and Flora expeditions (Raitt and others, 1967, 1969). The calculated curves for the North Arm Massif have been shifted so that all the curves are symmetrical about an azimuth of 90°. The agreement between the calculated and observed seismic anisotropy patterns is striking. Furthermore, this comparison allows us to estimate the volume percentages of olivine in the upper mantle underlying these regions at 70% and 100% in the Quartet and Flora areas, respectively. The estimates are, however, only correct if olivine and orthopyroxene are the major constituents of the upper mantle within these regions and the fabrics are similar to those observed in this study.

ACKNOWLEDGMENTS

This research was supported by the Office of Naval Research Contract N-00014-80-C-0252. The help of R. Carlson, R. Crosson, R. Ramananantoandro, and M. Salisbury in various aspects of this study is greatly appreciated.

REFERENCES CITED

Avé Lallemant, H. G., 1976, Structure of the Canyon Mountain (Oregon) ophiolite complex and its implication for sea-floor spreading: Geological Society of America Bulletin Special Paper 173, 49 p.

Babuska, V., 1972, Elasticity and anisotropy of dunite and bronzite: Journal of Geophysical Research, v. 77, p. 6955–6965.

Backus, G. E., 1965, Possible forms of seismic anisotropy of the uppermost mantle under oceans: Journal of Geophysical Research, v. 70, p. 3429–3439.

Baker, D. W., and Carter, N. L., 1972, Seismic velocity anisotropy calculated for ultramafic minerals and aggregates, *in* Heard, H. C., and others, eds., Flow and fracture of rocks: Washington, D.C., American Geophysical Union Geophysical Monograph, v. 16, p. 157–166.

Bamford, D., 1977, P_n velocity anisotropy in a continental upper mantle: Royal Astronomical Society Geophysical Journal, v. 49, p. 29–48.

Bamford, D., Jentsch, M., and Prodehl, C., 1979, P_n anisotropy studies in northern Britain and the eastern and western United States: Royal Astronomical Society Geophysical Journal, v. 57, p. 397–430.

Birch, F., 1960, The velocity of compressional waves in rocks to 10 kilobars, 1: Journal of Geophysical Research, v. 65, p. 1083–1102.

Brothers, R. N., and Rodgers, K. A., 1969, Petrofabric studies of ultramafic nodules from Auckland, New Zealand: Journal of Geology, v. 77, p. 452–465.

Carter, N. L., Baker, D. W., and George, R. P., Jr., 1972, Seismic anisotropy, flow, and constitution of the upper mantle, *in* Heard, H. C., and others, eds., Flow and fracture of rocks: Washington, D.C., American Geophysical Union Geophysical Monograph, v. 16, p. 167–190.

Christensen, N. I., 1966a, Elasticity of ultrabasic rocks: Journal of Geophysical Research, v. 71, p. 5921–5931.

—— 1966b, Shear wave velocities in metamorphic rocks at pressures to 10 kilobars: Journal of Geophysical Research, v. 71, p. 3549–3556.

—— 1970, Shear wave propagation in rocks, Nature, v. 229, p. 549–550.

Christensen, N. I., and Crosson, R. S., 1968, Seismic anisotropy in the upper mantle: Tectonophysics, v. 6, p. 93–107.

Christensen, N. I., and Salisbury, M. H., 1979, Seismic anisotropy in the oceanic upper mantle: Evidence from the Bay of Islands ophiolite complex: Journal of Geophysical Research, v. 84, p. 4601–4610.

Crampin, S., 1977, A review of the effects of anisotropic layering on the propagation of seismic waves: Royal Astronomical Society Geophysical Journal, v. 49, p. 9–27.

Crosson, R. S., and Lin, J. W., 1971, Voigt and Reuss prediction of anisotropic elasticity of dunite: Journal of Geophysical Research, v. 76, p. 570–578.

Deer, W. A., Howie, R. A., and Zussman, J., 1976, An introduction to the rock-forming minerals: London, Longman Group Limited, 528 p.

den Tex, E., 1969, Origin of ultramafic rocks, their tectonic setting and history: A contribution to the discussion of the paper, "The origin of ultramafic and ultrabasic rocks," by P. J. Wyllie: Tectonophysics, v. 7, p. 457–488.

Emmons, R. C., 1943, The universal stage: New York, Geological Society of America Memoir 8, 205 p.

Francis, T.J.G., 1969, Generation of seismic anisotropy in the upper mantle along the mid-oceanic ridges: Nature, v. 221, p. 162–165.

Frisillo, A. L., and Barsch, G. R., 1972, Measurement of single-crystal elastic constants of bronzite as a function of pressure and temperature: Journal of Geophysical Research, v. 77, no. 32, p. 6360–6384.

George, R. P., Jr., 1978, Structural petrology of the Olympus ultramafic complex in the Troodos ophiolite, Cyprus: Geological Society of America Bulletin, v. 89, p. 845–865.

Helmstaedt, H., and Anderson, O. L., 1969, Petrofabrics of mafic and ultramafic inclusions from kimberlite pipes in southeastern Utah and northeastern Arizona [abs.]: EOS Transactions, American Geophysical Union, v. 50, p. 345.

Hess, H. H., 1964, Seismic anisotropy of the uppermost mantle under oceans: Nature, v. 203, p. 629–631.

Klima, K., and Babuska, V., 1968, A comparison of measured and calculated elastic anisotropies of marble: Studies of Geophysics and Geodetics, v. 12, p. 377–384.

Kumazawa, M., 1964, The elastic constants of rock in terms of elastic constants of constituent mineral grains, petrofabric and interface structures: Journal of the Earth Sciences, Nagoya University, v. 72, p. 147–176.

Kumazawa, M., and Anderson, O. L., 1969, Elastic moduli, pressure derivatives and temperature derivatives of single crystal olivine and single crystal forsterite: Journal of Geophysical Research, v. 74, p. 5961–5972.

Loney, R. A., and Himmelberg, G. R., 1976, Structure of the Vulcan Peak alpine-type peridotite, southwestern Oregon: Geological Society of America Bulletin, v. 87, p. 259–274.

Morris, G. B., Raitt, R. W., and Shor, G. G., 1969, Velocity anisotropy and delay-time maps of the mantle near Hawaii: Journal of Geophysical Research, v. 74, p. 4300–4316.

Nicolas, A., and Poirier, J. P., 1976, Crystalline plasticity and solid state flow in metamorphic rocks: New York, John Wiley & Sons, 437 p.

Nicolas, A., Bouchez, J. L., Boudier, F., and Mercier, J. C., 1971, Textures, structures and fabrics due to solid state flow in some European lherzolites: Tectonophysics, v. 12, p. 55–86.

Nicolas, A., Boudier, F., and Bouchez, J. L., 1980, Interpretation of peridotite structures from ophiolitic and oceanic environments: American Journal of Science, v. 280-A, p. 192–210.

Raitt, R. W., Shor, G. G., Jr., Francis, T.J.G., and Morris, G. B., 1967, Anisotropy of the Pacific upper mantle: S10 Reference 67-8, Marine Physical Laboratory, Scripps Institute of Oceanography, San Diego, California, 42 p.

—— 1969, Anisotropy of the Pacific upper mantle: Journal of Geophysical Research, v. 74, p. 3095–3109.

Raitt, R. W., Shor, G. G., Jr., Morris, G. B., and Kirk, H. K., 1971, Mantle anisotropy in the Pacific Ocean: Tectonophysics, v. 12, p. 173–186.

Raleigh, C. B., 1965, Structure and petrology of an alpine peridotite on Cypress Island, Washington, U.S.A.: Contributions to Mineralogy and Petrology, v. 2, p. 719–741.

Ringwood, A. E., 1966, Mineralogy of the mantle, *in* Hurley, P. M., ed., Advances in earth science: Cambridge, Massachusetts, Massachusetts Institute of Technology Press, p. 357–399.

Ross, C. J., Foster, M. D., and Myers, A. T., 1954, Origin of dunites and olivine-rich inclusions in basaltic rocks: American Mineralogist, v. 39, p. 693–737.

Salisbury, M. H., and Christensen, N. I., 1978, The seismic velocity structure of a traverse through the Bay of Islands ophiolite complex, Newfoundland, an exposure of oceanic crust and upper mantle: Journal of Geophysical Research, v. 83, p. 805–817.

Smith, C. H., 1958, Bay of Islands igneous complex, western Newfoundland: Canada Geological Survey Memoir, v. 290, 132 p.

Verma, R. K., 1960, Elasticity of some high density crystals: Journal of Geophysical Research, v. 65, p. 757–766.

Williams, H., 1971, Mafic-ultramafic complexes in western Newfoundland Appalachians and the evidence for transportation: A review and interim report: Geological Association of Canada, Proceedings v. 24, p. 9–25.

—— 1973, The Bay of Islands map area, Newfoundland: Canada Geological Survey Paper 72-34, p. 1–7.

Manuscript Received by the Society March 2, 1981
Revised Manuscript Received June 8, 1981
Manuscript Accepted June 23, 1981